International Journal of Biological Macromolecules 282 (2024) 136821

Contents lists available at ScienceDirect

International Journal of Biological Macromolecules

journal homepage: www.elsevier.com/locate/ijbiomac

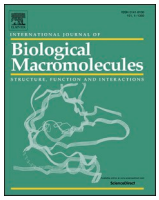

Preventing osteoporotic bone loss in mice by promoting balanced bone remodeling through M-CSF$_{RGD}$, a dual antagonist to c-FMS and αvβ3 receptors

Yuval Zur [a,1], Svetlana Katchkovsky [b,1], Amit Itzhar [a], Chen-Viki Abramovitch-Dahan [b], David Stepensky [c], Niv Papo [a,*], Noam Levaot [b,*]

[a] Avram and Stella Goldstein-Goren Department of Biotechnology Engineering, Ben-Gurion University of the Negev, Beer-Sheva 8410501, Israel
[b] Department of Physiology and Cell Biology, Faculty of Health Sciences, Ben-Gurion University of the Negev, Beer-Sheva 8410501, Israel
[c] Department of Clinical Biochemistry and Pharmacology, Faculty of Health Sciences, Ben-Gurion University of the Negev, Beer-Sheva 8410501, Israel

ARTICLE INFO

Keywords:
Osteoporosis
M-CSF
αvβ3 integrin
c-FMS
Bone metabolism
Osteoclast

ABSTRACT

Osteoporosis is a common, age-related disease caused by imbalanced bone remodeling. Current treatments either shut down bone resorption or robustly stimulate bone formation. Here, we describe a novel compound that inhibits osteoclast activity without causing apparent disruptions to bone formation by targeting both c-FMS (*i.e.*, osteoclast differentiation) and αvβ3 integrin (*i.e.*, osteoclastic bone resorption) receptors. We show that human serum albumin (HSA)-conjugated M-CSF$_{RGD}$ protein (M-CSF$_{RGD}$-HSA) effectively inhibits the activity of both receptors, with a three-fold higher serum half-life compared to the unconjugated M-CSF$_{RGD}$. We then treated ovariectomized mice with different doses of M-CSF$_{RGD}$-HSA, alendronate, or a monospecific control protein. The bispecific M-CSF$_{RGD}$-HSA was superior to a monospecific control in alleviating bone loss and reducing osteoclast distribution and function. M-CSF$_{RGD}$-HSA and alendronate effectively prevented ovariectomy-induced bone loss, but M-CSF$_{RGD}$-HSA had a milder inhibitory effect on osteoclast distribution and activity. Moreover, alendronate halted bone formation, while M-CSF$_{RGD}$-HSA-treated mice showed an increased level of serum amino-terminal propeptide of type I collagen, a bone formation marker. Our data indicate that the mild reduction in osteoclast activity facilitated by the bispecific M-CSF$_{RGD}$-HSA allows the maintenance of certain levels of bone formation and may be superior to treatments that induce osteoclast depletion.

1. Introduction

Osteoporosis, a common, age-related skeletal disease, develops as a result of an imbalanced bone remodeling process. With aging, at a certain point, the amount of bone tissue resorbed by osteoclasts exceeds the amount of bone tissue formed by osteoblasts. Inevitably, this disproportional activity causes loss of bone mass, increased fragility, and a tendency to fracture [1,2].

Osteoporosis is vastly underdiagnosed and causes a significant reduction in quality of life and life expectancy in a rapidly growing affected population [3]. Currently available antiresorptive and anabolic therapeutics (*e.g.*, bisphosphonates, teriparatide) provide robust effects in shutting down resorption or stimulating bone formation. The disproportionate effects of these drugs on bone resorption or bone formation, although effective in reducing fracture rates for a few years [4–7], do not restore the bone remodeling balance. The artificial perturbations in bone remodeling balance limit long-term usage of the drugs due to a reduction in efficacy [8] and, in some cases, the appearance of serious side effects such as hypo/hypercalcemia, osteonecrosis of the jaw [9] and atypical fractures [10,11]. Therefore, there is a great need for safe drugs that will restore bone remodeling balance and could serve for prolonged treatment or even as a preventive measure for osteoporosis.

Proof of concept of the feasibility to inhibit bone resorption while preserving bone formation was provided by the clinical studies of the cathepsin K inhibitor odanacatib. Odanacatib was shown to be effective in inhibiting osteoclast-mediated bone resorption. However, odanacatib did not entirely eliminate osteoclasts, hence permitting ongoing

* Corresponding authors.
E-mail addresses: papo@bgu.ac.il (N. Papo), levaot@bgu.ac.il (N. Levaot).
[1] Equal contribution.

https://doi.org/10.1016/j.ijbiomac.2024.136821
Received 23 June 2024; Received in revised form 13 October 2024; Accepted 21 October 2024
Available online 22 October 2024

signaling by osteoclasts to promote bone formation [12]. In clinical trials odanacatib effectively increased bone mineral density and reduced risk of fracture [13]. Nevertheless, it also increased risk of cardiovascular events by an unknown mechanism, and its development was thus discontinued [14]. Thus, although discontinued, odanacatib serves as an indication that it is possible to inhibit osteoclast cells resorption activity without disrupting a normal bone remodeling cycle.

For osteoclasts to differentiate, two events are required and sufficient: progenitor cells exposure to soluble macrophage colony stimulating factor (M-CSF) which binds to c-FMS receptor tyrosine kinase, and subsequent exposure of the progenitors to the receptor activator of NF-κB ligand (RANKL) cytokine [15]. On the other hand, extensive number of factors are required for osteoclasts to gain proper resorptive activity [16–18]. One of these factors is αvβ3 integrin, which regulates osteoclast cytoskeleton organization, migration, adhesion to bone and formation of the sealing zone [19,20].

It was shown previously that bone marrow macrophages (BMMs) from $\beta3^{-/-}$ mice differentiate into osteoclasts (*i.e.*, multinuclear cells), which fail to spread properly. Subsequently, $\beta3^{-/-}$ mice exhibit osteosclerotic phenotype (*i.e.*, increased cortical and trabecular bone mass and density) with increased number of osteoclasts but defective resorptive capacity [21]. In addition, this phenotype is characterized by significantly increased M-CSF levels in mice serum and bone marrow. Intriguingly, *in vitro* studies show that high dose of recombinant M-CSF rescues $\beta3^{-/-}$ osteoclast progenitors' maturation and spreading, and the cells morphology appears normal. However, the resorptive function is not restored in these cells and they are, essentially, inactive [22]. Taken together, these findings indicate that c-FMS and αvβ3 integrin work in concert and complement each other in obtaining normal osteoclast differentiation and function.

Inspired by this observation, in our previous work [23] we described a novel approach for inhibiting osteoclast differentiation and activity by dual targeting of c-FMS and αvβ3 integrin. The bispecific protein developed by our team, termed M-CSF_{RGD}, exhibited high specificity and bound both receptors with nanomolar (nM) binding affinities (96 nM for c-FMS and 245 nM for αvβ3 integrin). We demonstrated that M-CSF_{RGD} binds specifically to αvβ3 integrin and not to any other integrin family members. Furthermore, it effectively inhibited both c-FMS and αvβ3 integrin signaling. *In vitro*, it was superior in inhibiting osteoclast cytoskeletal organization and differentiation compared to monospecific control proteins that target only c-FMS or αvβ3 integrin. Moreover, the level of bone resorption marker Collagen Type 1 C-Telopeptide (CTX—I) was significantly reduced in mice injected subcutaneously (SC) with the bispecific protein, compared to the vehicle-injected group.

The major goal of the current study is to determine whether dual targeting of c-FMS and αvβ3 could serve as a treatment for osteoporosis through a reduction in the level of bone resorption by osteoclasts without tampering with the coupling between resorption and formation processes. Here, we show that conjugation of M-CSF_{RGD} to human serum albumin (M-CSF_{RGD}-HSA) improves its biodistribution and accumulation in the bone tissue. Treatment of ovariectomized mice with M-CSF_{RGD}-HSA effectively inhibits bone resorption without evident interruption of bone formation and prevents osteoporotic bone loss.

2. Results

2.1. Engineering M-CSF_{RGD} with improved bioavailability and pharmacokinetic properties

Previously, we showed that SC injection of M-CSF_{RGD} protein twice a day for three days reduced the serum levels of CTX-I in mice, indicating effective inhibition of bone resorption *in vivo*. Moreover, by fluorescent imaging performed 3 h (hr) post-injection, the M-CSF_{RGD} signal was observed in the long bones of mice but not in other major organs. However, SC-injected M-CSF_{RGD} was rapidly accumulated in the mouse kidneys and gallbladder and was completely cleared from the mouse body following 6 h of injection [23]. This comes in agreement with the well-described inverse correlation between protein size (M-CSF_{RGD} is only 21 kDa in size) and an expected systemic clearance within only 3–5 h for such a small protein [24–26]. Thus, to achieve the utmost effect on bone metabolism by targeting c-FMS and αvβ3 integrin *in vivo*, there was a need to improve the pharmacokinetic properties of the bispecific M-CSF_{RGD}.

For this purpose, the bispecific M-CSF_{RGD} and its c-FMS-targeting monospecific control, M-$CSF_{c\text{-}FMS}$, were each fused with HSA *via* the C-terminal region. This step is a well-established strategy to extend protein half-life due to both the interaction with the neonatal Fc receptor recycling system and a slower clearance by the renal system, thus allowing for a prolonged therapeutic effect [27,28]. Linker peptides (GGGGS) were added to the final protein construct to allow spatial separation between the fused domains (Figs. 1a and S1), aimed at preserving the biological activity [29,30]. This resulted in 92 kDa fusions, namely a bispecific M-CSF_{RGD}-HSA and a monospecific M-$CSF_{c\text{-}FMS}$-HSA.

To validate that the fusion to HSA did not affect the activity of the proteins (*i.e.*, inhibition of osteoclast differentiation), mouse BMMs were cultured with soluble M-CSF and RANKL to induce differentiation in the presence or absence of different concentrations of the fusion proteins. Treatment with M-CSF_{RGD} or M-CSF_{RGD}-HSA resulted in a drastic reduction of osteoclast number, nuclei number, and osteoclast area (Fig. 1b-d), compared to untreated cells. Similarly, both M-$CSF_{c\text{-}FMS}$ and M-$CSF_{c\text{-}FMS}$-HSA showed significant inhibition of osteoclast differentiation compared to the positive control. Moreover, the highest concentration of M-$CSF_{c\text{-}FMS}$-HSA (1 μM) was more effective than the highest concentration of M-$CSF_{c\text{-}FMS}$ (5 μM) in reducing the area and number of osteoclasts, as well as the number of the nuclei (Fig. S2a-c). Taken together, these data demonstrate that fusion of M-CSF_{RGD} or M-$CSF_{c\text{-}FMS}$ with HSA does not disturb their inhibitory effect on osteoclast differentiation *in vitro*. Since osteoclast and osteoblast activity in bone are tightly coupled, we aimed to assess the impact of the fusion of M-CSF_{RGD} with HSA on osteoblasts as well.

Previously, we have shown that M-CSF_{RGD} does not affect the survival or proliferation of murine bone marrow-derived mesenchymal stromal cells (BMSCs) [23]. To determine whether the fusion of M-CSF_{RGD} with HSA affects osteoblast differentiation, we evaluated the formation of mineralized nodules in cultures of the MC3T3 osteoblastic cell line treated with different concentrations of M-CSF_{RGD}-HSA. Treatment of the cells with 50 or 250 nM M-CSF_{RGD}-HSA resulted in an increase in the number of mineralization nodules (Fig. S3).

To determine whether the HSA addition improves biodistribution and accumulation of the fusion proteins in bone tissue, M-CSF_{RGD}-HSA and M-CSF_{RGD} were conjugated to a fluorescent dye and administered to mice *via* a single SC injection. One-hour post-injection, M-CSF_{RGD}, but not M-CSF_{RGD}-HSA, was accumulated in the kidneys (Fig. 2a), with no detectable signals in the heart, lungs, liver, intestines, or spleen. M-CSF_{RGD} was cleared from the body 24 h post-injection, as opposed to M-CSF_{RGD}-HSA, which was still detected in the femur (Fig. 2b). Moreover, a strong signal from M-CSF_{RDG}-HSA could be detected in bones even one week after injection (Fig. 2c).

Our next aim was to determine whether the fusion with HSA improves pharmacokinetic properties and, specifically, the elimination half-life of the protein. Therefore, a single dose of 10 mg/kg of a protein was administered to BALB/c mice *via* either an IV injection (M-CSF_{RGD}-HSA or M-CSF_{RGD}) or a SC injection (M-CSF_{RGD}-HSA). The mouse serum was collected at different time points, and the concentration of the full-length proteins was determined using a sandwich enzyme-linked immunosorbent assay (ELISA) consisting of antibodies that target N- and C-terminal tags (FLAG and His, respectively) of the proteins.

Following the IV administration, M-CSF_{RGD} serum concentrations declined rapidly in an exponential fashion and reached undetectable levels within 6 h (Fig. 2d). On the other hand, the M-CSF_{RGD}-HSA concentration *vs.* time curve exhibited more complex, presumably three-compartmental, pharmacokinetic behavior. Initial rapid decline (the

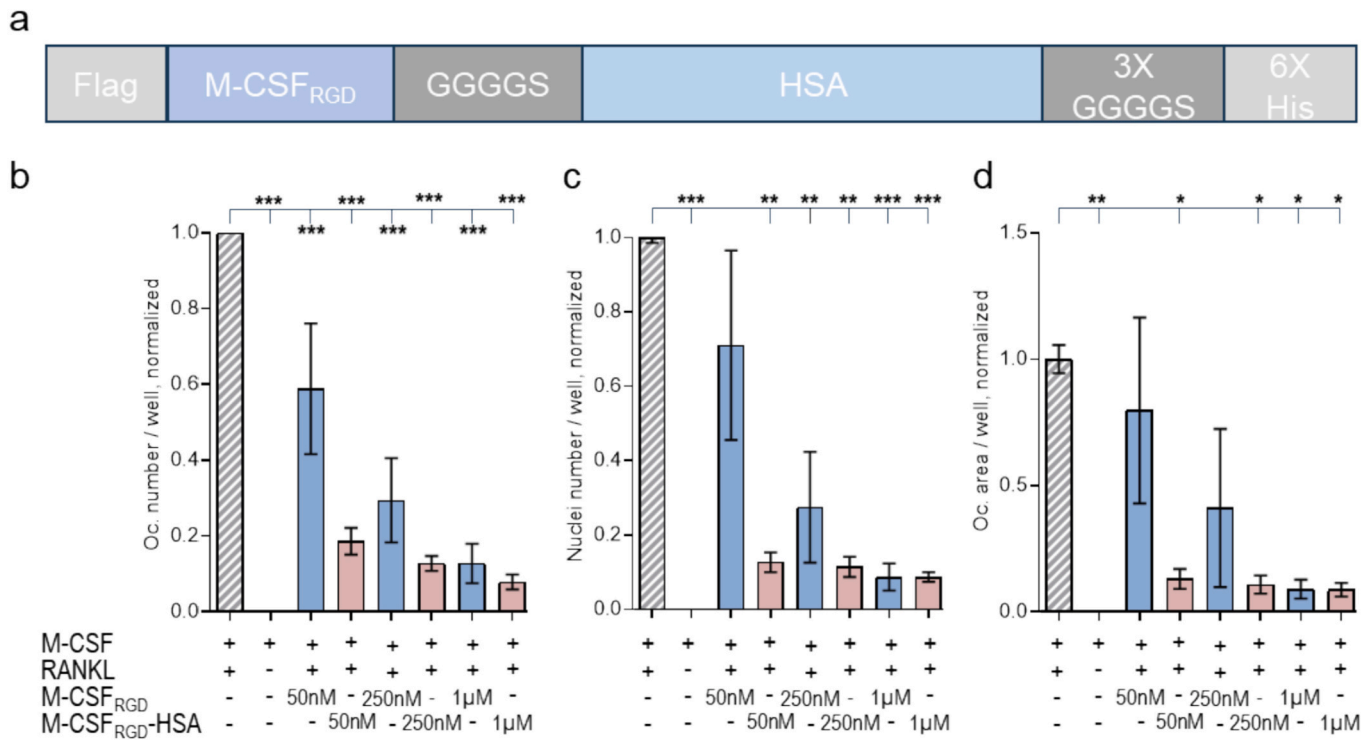

Fig. 1. M-CSF$_{RGD}$ fused to HSA preserves the inhibitory activity on osteoclast differentiation *in vitro* (a) Schematic representation of the final construct for M-CSF$_{RGD}$ or M-CSF$_{c\text{-}FMS}$ fusion with HSA. (b-d) Osteoclast differentiation assay. Quantitative data of tartrate-resistant acid phosphatase (TRAP)-positive multinucleated cells derived from mouse BMMs by stimulation with 20 ng/ml of M-CSF and RANKL. The cells were treated with different concentrations of recombinant purified M-CSF$_{RGD}$ or M-CSF$_{RGD}$-HSA for 4 days and analyzed for (b) the number of osteoclasts per well (Oc. number/well), (c) the number of nuclei per well, and (d) the osteoclast area per well (Oc. area/well). All values were normalized to control differentiated, untreated osteoclasts. The data are presented as means ± SEM of triplicates.

distribution phase) during the first 6 h was followed by slower elimination phases, and the terminal half-life was ~25-fold higher compared to that of M-CSF$_{RGD}$ (15.03 *vs.* 0.597 h; Fig. 2e). The area under the curve ($AUC_{0\text{-}\infty}$) of M-CSF$_{RGD}$-HSA was 3.84-fold higher, relative to that of M-CSF$_{RGD}$ (177.9 μg·h/mL and 46.3 μg·h/mL, respectively). This increase in the systemic exposure of the M-CSF$_{RGD}$-HSA fusion protein is apparently due to its lower volume of distribution and lower clearance compared to M-CSF$_{RGD}$.

Following the SC injection, M-CSF$_{RGD}$-HSA serum concentrations increased gradually during the first 6 h, followed by a gradual, prolonged decline. The terminal half-life of SC of M-CSF$_{RGD}$-HSA was somewhat longer compared to the IV administration (19.1 h *vs.* 15.03 h; Fig. 2e); however, a decisive conclusion regarding the flip-flop pharmacokinetics of SC M-CSF$_{RGD}$-HSA (*i.e.*, the terminal half-life represents the absorption kinetics of the fusion protein from the SC administration site) cannot be reached based on the available data. The absolute bioavailability of M-CSF$_{RGD}$-HSA by the SC route was 59.5 % (105.8 μg·h/mL/177.9 μg·h/mL·100 %; see the AUC data, Fig. 2e), which is appropriate and plausible for a 92 kDa protein [31,32].

Overall, the HSA conjugation substantially improved the pharmacokinetic behavior of M-CSF$_{RGD}$, increased the systemic exposure, and dramatically prolonged the terminal half-life. The SC administration of M-CSF$_{RGD}$-HSA was somewhat inferior to that of the IV administration route (59.5 % bioavailability, *i.e.*, loss of ~40 % of the injected protein conjugate). Despite this, we decided to use the SC route for M-CSF$_{RGD}$-HSA administration in the subsequent *in vivo* experiments. This is because a SC drug administration is more convenient and less painful for patients, and it carries a lower risk of infection compared to the IV and intraperitoneal injection (IP) administration routes [33]. Moreover, SC injections can be self-administered by the patients, resulting in more convenient and cost-effective treatment regimens for many biologicals and some non-biological drugs [34].

2.2. M-CSF$_{RGD}$-HSA prevents vertebral bone loss in ovariectomized mice

To determine whether the bispecific M-CSF$_{RGD}$-HSA could prevent osteoporosis-associated bone loss, we used a mouse model of postmenopausal osteoporosis induced by ovariectomy. The mice were SC injected with either phosphate-buffered saline (PBS), M-CSF$_{RGD}$-HSA (2.5 or 10 mg/kg), or M-CSF$_{c\text{-}FMS}$-HSA (10 mg/kg) twice a week for 3 weeks. This dosing frequency was chosen based on the shape of the pharmacokinetic curve of the HSA conjugate (Fig. 2d) and an expectation of maintaining its pharmacologically relevant systemic concentrations for at least 3–4 days after each injection. Alendronate, an FDA-approved bisphosphonate for treatment of postmenopausal osteoporosis [35], was injected in the same manner at a 0.1 mg/kg dose to a control group. No significant distress was caused to mice by the surgery, as confirmed by the absence of a change in body weight throughout the treatment duration (Fig. S4a). The ovariectomy procedure was successful, confirmed by weighing the uteri after sacrificing the mice to validate uterine atrophy (Fig. S4b).

Analysis of femoral cortical bone parameters did not show any significant changes between the ovariectomized (OVX) mice and the sham-operated control, as well as between any of the treatment groups and the control groups (Fig. S5). As expected, the OVX mice displayed a significant reduction in trabecular bone volume, trabecular number, and thickness compared to the sham-operated control group, as revealed by a micro-computed tomography (μCT) analysis of the extracted vertebrae (Fig. 3a–d). The mice treated with alendronate displayed a significant increase in trabecular bone volume, trabecular number, and thickness, as expected (Fig. 3a-c) [36–38].

Similarly to alendronate, the bispecific M-CSF$_{RGD}$-HSA prevented ovariectomy-induced bone loss by increasing the bone volumetric parameters. The 2.5 mg/kg dose's effect (termed the low dose) was statistically significant, while the 10 mg/kg dose (termed the high dose)

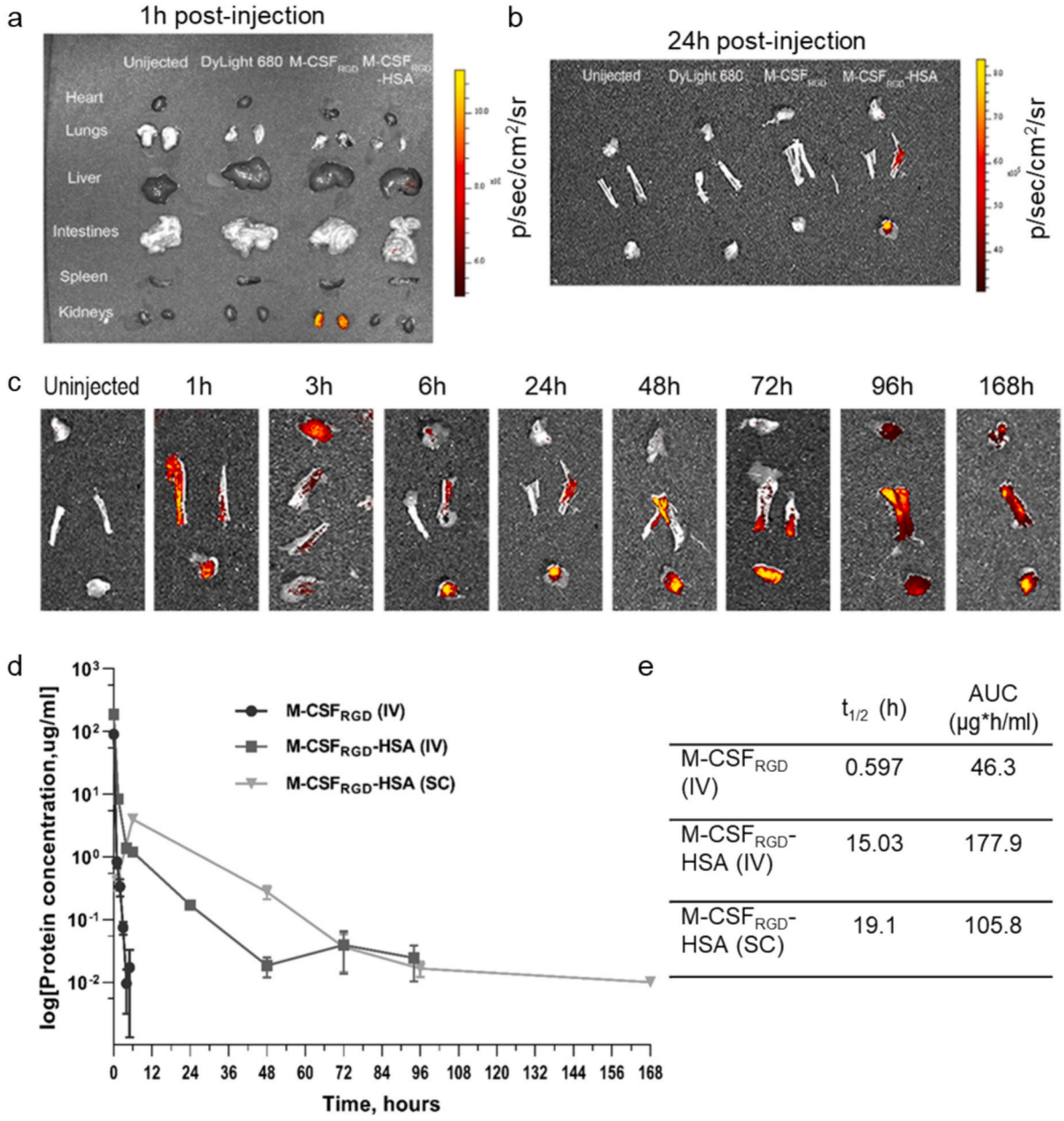

Fig. 2. M-CSF$_{RGD}$ fusion with HSA significantly improves the pharmacokinetic properties (a-c) *In vivo* fluorescence imaging of the major organs of BALB/c mice after a SC injection of M-CSF$_{RGD}$ or M-CSF$_{RGD}$-HSA conjugated to DyLight 680 at various predetermined post-injection time periods. (a) Images of internal organs one-hour post-injection; (b) Images of the right femur 24 h post-injection; and (c) Images of both femurs at different time points in mice injected with M-CSF$_{RGD}$-HSA conjugated to DyLight 680 or uninjected control mice. (d) Serum concentration *vs.* time data after 10 mg/kg single IV injection of M-CSF$_{RGD}$-HSA and M-CSF$_{RGD}$ ($n = 4$), and SC injection of M-CSF$_{RGD}$-HSA ($n = 3$) to BALB/c mice. Protein concentration in serum was determined using sandwich ELISA with antibodies targeting the N- and C-terminal tags of the protein constructs. The data are presented as means ± SD. (e) The results of non-compartmental pharmacokinetic analysis (the mean values of the terminal half-life and the area under the curve).

also prevented bone loss by a close-to-significant value ($p = 0.0696$). Of note, mice treated with the low M-CSF$_{RGD}$-HSA dose had the highest mean bone volume fraction among all treated groups, including the well-established antiresorptive drug alendronate-treated group (Fig. 3a). As opposed to the treatment with the bispecific proteins, the monospecific M-CSF$_{c\text{-}FMS}$-HSA failed to prevent ovariectomy-induced bone loss (Fig. 3a).

The effect on trabecular architecture varied between the tested concentrations of M-CSF$_{RGD}$-HSA. The high dose showed a significant increase in trabecular number but did not affect trabecular thickness (Fig. 3b-d). The low dose led to a significant increase both in trabecular bone number and thickness and was the only treatment that displayed a close-to-significant change in trabecular separation ($p = 0.0524$ *vs.* OVX group), supporting its superiority over the other treatments (Fig. 3b-d). Taken together, our data demonstrate that targeting both c-FMS and αvβ3 integrin is more effective than targeting c-FMS alone in the prevention of osteoporotic bone loss.

2.3. M-CSF$_{RGD}$-HSA inhibits bone resorption without causing a decline in bone formation marker level

To further explore the mechanisms underlying the superior effect of the bispecific M-CSF$_{RGD}$-HSA in the prevention of bone loss in OVX mice, we compared bone turnover markers between the different groups. As

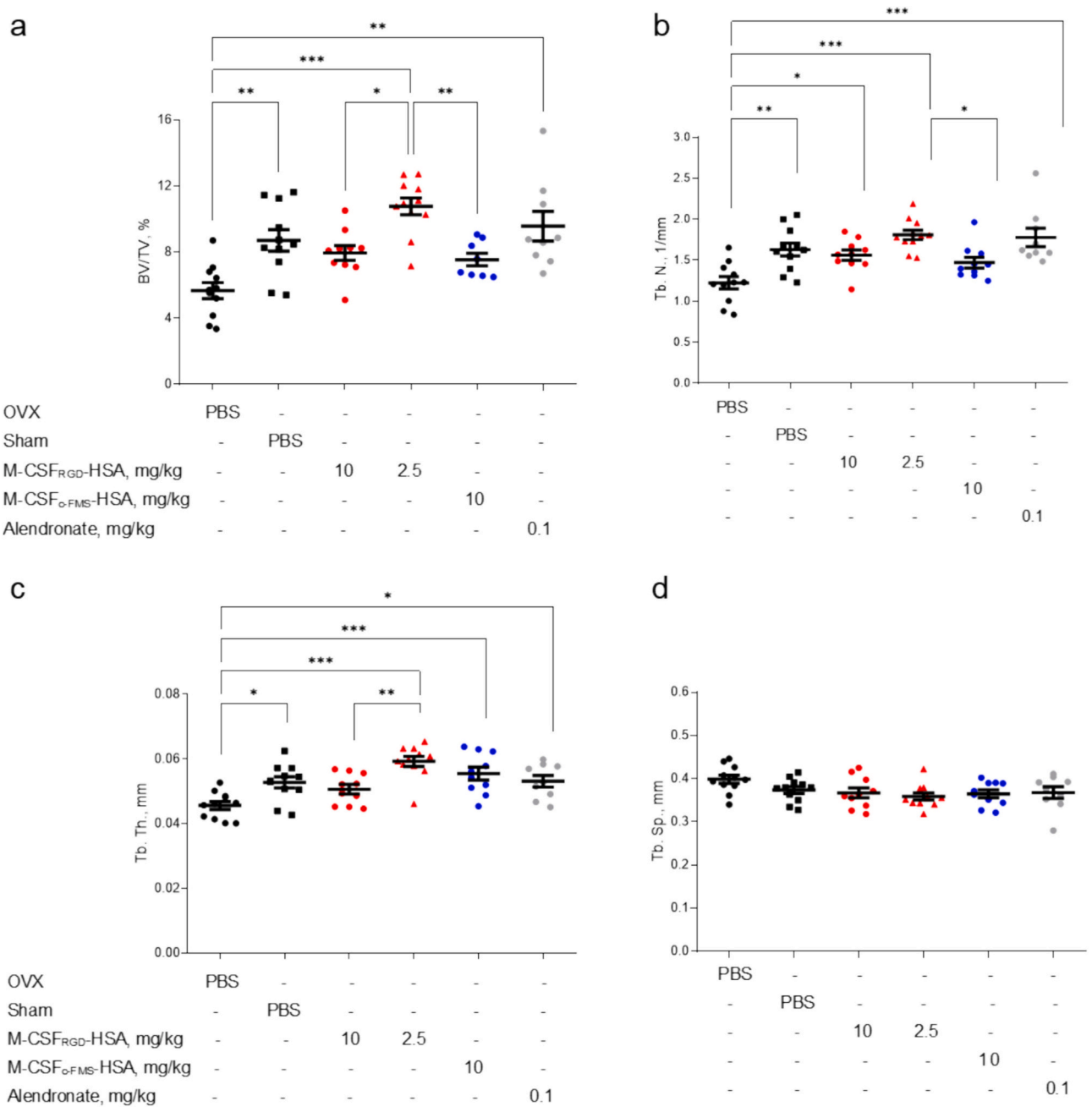

Fig. 3. Treatment with recombinant M-CSF$_{RGD}$-HSA prevents trabecular bone loss in ovariectomized mice Thirteen-week-old female OVX or sham-operated BALB/c mice were treated with different concentrations of either M-CSF$_{RGD}$-HSA (2.5 or 10 mg/kg), M-CSF$_{c\text{-}FMS}$-HSA (10 mg/kg), or alendronate (0.1 mg/kg) for 3 weeks with bi-weekly SC injections. (a-d) Vertebral μCT analysis of trabecular bone parameters in terms of (a) bone volume as a percentage of total trabecular volume (BV/TV), (b) trabecular number (Tb. N), (c) thickness (Tb. Th), and (d) separation (Tb. *Sp.*). Data are means ± SEM of 10 or 11 mice per group.

expected, the ovariectomy procedure induced high bone resorption, reflected by an increase in CTX-I level compared to the sham-operated mice [39]. Treatment with the monospecific M-CSF$_{c\text{-}FMS}$-HSA had no effect on CTX-I levels. Treatment with either alendronate or the high dose of M-CSF$_{RGD}$-HSA significantly reduced the level of CTX-I (Fig. 4a). Interestingly, despite the positive effects of treatment with the low dose of M-CSF$_{RGD}$-HSA on bone volume, its effect on CTX-I level was mild and did not reach a statistically significant value.

To further examine the effect of treatment with monospecific *vs.* bispecific M-CSF$_{RGD}$-HSA on bone resorption, histological sections of vertebrae were stained with TRAP and analyzed for osteoclast number and perimeter. As expected, ovariectomy significantly and profoundly increased osteoclast number and perimeter compared to the sham-operated control group (Fig. 4b-c). In all the treatment groups, a significant reduction in the osteoclast number and perimeter was observed. Furthermore, with M-CSF$_{RGD}$-HSA, this effect was achieved in a dose-dependent manner (Fig. 4b-c, e).

As for bone formation, in the majority of the treatment groups, the ovariectomy-induced increase in the mean value of the serum amino-terminal propeptide of type I collagen (PINP) level was not significant compared to the sham-operated group. Among all the different treatments, only the bispecific M-CSF$_{RGD}$-HSA significantly elevated PINP levels (Fig. 4d). Notably, the low dose of M-CSF$_{RGD}$-HSA significantly increased bone formation compared to treatment with alendronate. Mice treated with alendronate had the lowest serum levels of PINP among all the experimental groups, accentuating the negative impact of

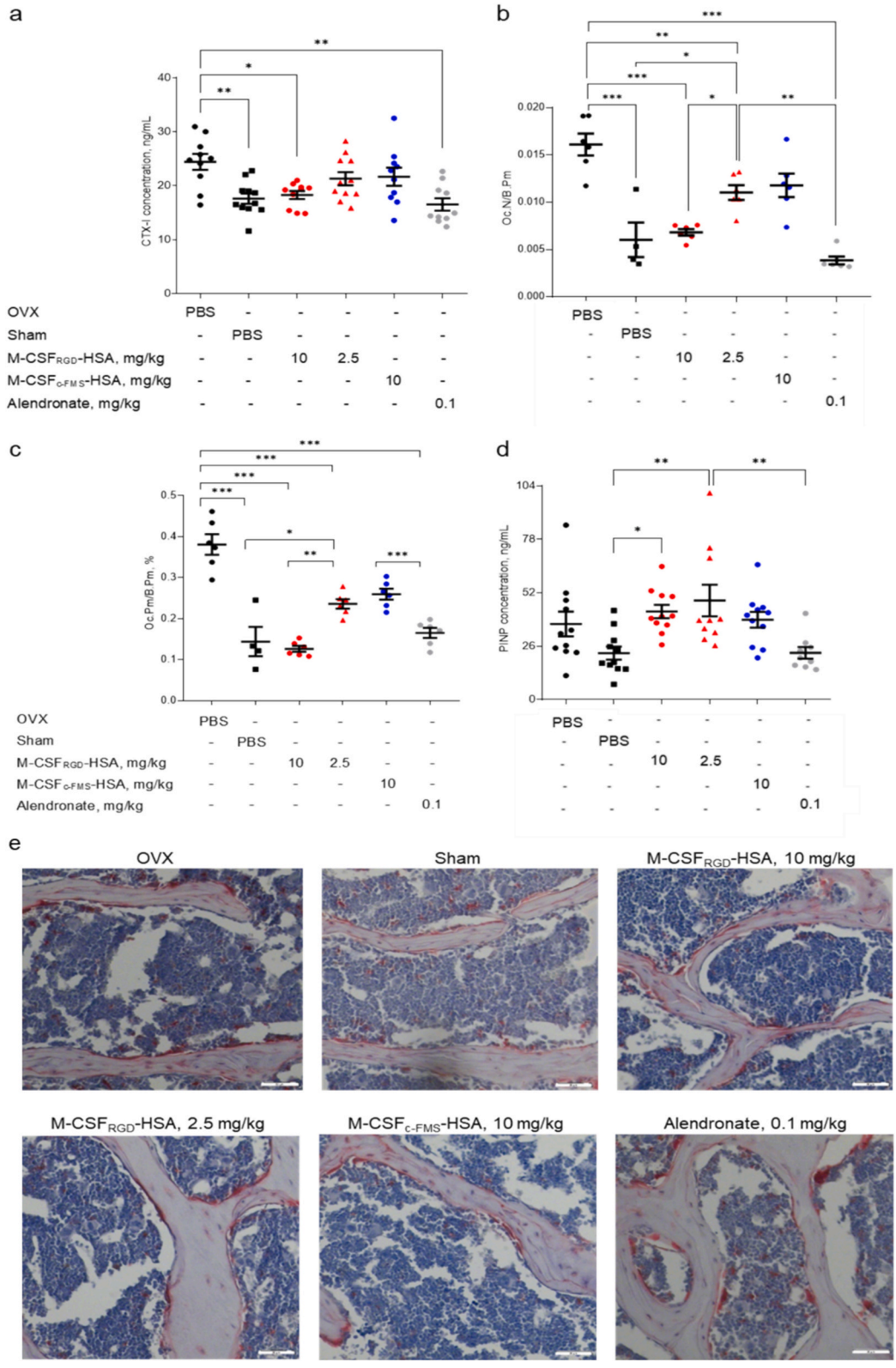

Fig. 4. M-CSF$_{RGD}$-HSA inhibits bone resorption without negative effects on the bone formation process Mice were sham-operated or ovariectomized, and SC injected with either PBS, M-CSF$_{RGD}$-HSA (2.5 or 10 mg/kg), M-CSF$_{c\text{-}FMS}$-HSA (10 mg/kg), or alendronate (0.1 mg/kg) twice a week for three weeks. Serum levels of (a) the bone resorption marker, CTX—I. (b-c) Histological analysis of TRAP-stained osteoclasts in vertebral sections: (b) osteoclast number per bone perimeter (Oc. N/B. Pm) and (c) osteoclast perimeter per bone perimeter (Oc. Pm/B. Pm). (d) Serum levels of the bone formation marker, PINP. The data are presented as mean ± SEM. Serum analysis was performed on 10–11 mice per group, and histological analysis was performed on six mice per group. (e) Representative images of TRAP-stained vertebrae of different treatment groups. Seven μm sections were imaged with a Zeiss microscope at ×20 magnification. Scale bar is 50 μm.

bisphosphonates on bone formation (Fig. 4d). As in the case of resorption (*i.e.*, CTX-I levels), the monospecific control targeting c-FMS failed to increase bone formation (*i.e.*, PINP levels), underscoring the superiority of simultaneous targeting of c-FMS and αvβ3 integrin.

3. Discussion

The current study aimed to elucidate whether it is feasible to treat osteoporosis by dual targeting of c-FMS and αvβ3 integrin, *i.e.*, inhibition of osteoclast resorptive function but not differentiation, thus potentially preserving consecutive osteoblast-mediated bone formation process. Furthermore, we sought to provide new insights and better understanding of regulation of bone remodeling by cooperation between c-FMS and αvβ3, by using the bispecific M-CSF$_{RGD}$ protein for *in vivo* treatment.

We show that the bioavailability of M-CSF$_{RGD}$ can be substantially enhanced without compromising its inhibitory activity in osteoclasts *in vitro*; this was achieved through conjugation of its C-terminal to HSA. In addition, we have shown that M-CSF$_{RGD}$-HSA fusion exerts a positive influence on osteoblast differentiation *in vitro*. Notably, albumin has been reported to enhance osteoblastic cell proliferation significantly *in vitro* [40] and to accelerate bone healing *in vivo* [41]. Thus, the positive effects of M-CSF$_{RGD}$-HSA on osteoblast differentiation may stem either from the HSA fusion or be attributable to a direct effect of M-CSF$_{RGD}$ through mechanisms that have yet to be identified.

We demonstrate a significant improvement in the pharmacokinetic profile of M-CSF$_{RGD}$ when fused to HSA. The terminal half-life of M-CSF$_{RGD}$-HSA is 15 h, which is 25 times longer than that of the unconjugated M-CSF$_{RGD}$. Nevertheless, the half-life is still shorter than that of murine serum albumin, which has a reported half-life of 35 h. The human equivalent, HSA, used in the current study has been found to have a lower affinity to mouse FcRn than mouse albumin [42]. Therefore, the shorter-then-expected half-life of M-CSF$_{RGD}$-HSA fusion in mice is likely a result of a less efficient recycling of the protein [43]. Nevertheless, our results show that M-CSF$_{RGD}$-HSA can be detected in the bones of injected mice for up to a week after a single injection. It is important to note that in humans, HSA has a serum circulation half-life of approximately three weeks [44]. This suggests that conjugating M-CSF$_{RGD}$ with HSA could significantly extend the systemic exposure in a clinical setting, making it a more attractive therapeutic choice for chronic patients. Thus, while improving the half-life of M-CSF$_{RGD}$ remains an ongoing objective, the current approach of fusing it with HSA provides a solid foundation for enhancing the duration of its therapeutic effects.

Our results show that injection of M-CSF$_{RGD}$-HSA, which effectively targets both M-CSF and αvβ3 integrin activity, prevents the ovariectomy-induced bone loss. To evaluate if this approach will outperform the targeting of only one of the receptors, we compared M-CSF$_{RGD}$-HSA activity to a c-FMS-targeting protein. Treatment with 10 mg/kg of the monospecific M-CSF$_{C\text{-}FMS}$-HSA resulted in a modest yet significant reduction in osteoclast number and perimeter. However, as opposed to the bispecific M-CSF$_{RGD}$-HSA, this reduction was not reflected by a lower CTX-I serum level nor by an elevation in trabecular bone volumetric parameters. We suggest that the superior effect of the bispecific inhibitor over targeting C-FMS alone could be derived from the monospecific protein's failure to shut off the redundant functions of both signaling pathways during osteoclast differentiation [45].

Bisphosphonates are the most common group of drugs utilized in the treatment of osteoporotic patients. Bisphosphonates strongly inhibit bone resorption, yet their uncontrolled, complete shutdown of bone remodeling limits their long-term safety and prolonged pharmacological application. Here, we compared the effects of treatment with M-CSF$_{RGD}$-HSA to a widely used bisphosphonate drug, alendronate. Previously, alendronate was shown to reduce the number of osteoclast precursors and to radically inhibit mature active osteoclasts [46,47], thus strongly impeding bone resorption. Alendronate also lowers bone turnover rate by delaying the onset of bone formation, possibly by interfering with the release of osteogenic signaling molecules by the osteoclasts [48]. In agreement with earlier findings, treatment with alendronate drastically reduced the number and perimeter of osteoclasts and lowered CTX-I serum levels, resulting in a net increase in vertebral bone volumetric parameters. The prevention of ovariectomy-induced bone loss was similar in the alendronate and M-CSF$_{RGD}$-HSA-treated groups. However, mice treated with alendronate had the lowest levels of the bone formation marker PINP compared to all treatment groups, while mice treated with M-CSF$_{RGD}$-HSA showed a significant increase in PINP levels, highlighting the distinct effects of alendronate and M-CSF$_{RGD}$-HSA on bone remodeling.

Of note, there was a difference between the effects of the two doses of the conjugate used in our study. Treatment with the high dose of M-CSF$_{RGD}$-HSA essentially reiterated the results observed in the alendronate-injected mice group. We suggest that this effect was achieved due to the high local concentration of the protein, which allowed potent inhibition of both osteoclast differentiation and activity. On the other hand, treatment with the low dose of M-CSF$_{RGD}$-HSA caused a substantial decrease in osteoclast number and perimeter compared to the OVX mouse group. However, the reduction was significantly milder than in 10 mg/kg M-CSF$_{RGD}$-HSA or alendronate-treated groups, which was also reflected by the absence of changes in serum CTX-I levels. We assume that this relatively mild inhibition of osteoclast resorption and not differentiation allowed the continuation of the bone remodeling flow, *i.e.*, recruitment of osteogenic cells *via* osteoclast signaling. Ultimately, the low dose of the bispecific M-CSF$_{RGD}$-HSA significantly enhanced trabecular bone volume, number, and thickness compared to the OVX mice group and groups treated with the monospecific M-CSF$_{C\text{-}FMS}$-HSA or high dose of M-CSF$_{RGD}$-HSA. Moreover, this protective effect on bone was more pronounced than that of alendronate.

For the first time, our data provide direct evidence that osteoclast differentiation and resorption activity *in vivo* depend on the crosstalk between c-FMS and αvβ3 integrin. However, the use of M-CSF$_{RGD}$-HSA as a long-term treatment for osteoporosis may not only inhibit osteoclasts but also macrophages by suppressing M-CSF–c-FMS signaling. This may raise concerns that innate immunity may also be suppressed in patients receiving M-CSF$_{RGD}$-HSA. However, we presume that the risk of immunosuppression is low, given the following observations: (1) M-CSF$_{RGD}$ is osteoclast-specific–the selectivity is achieved through a dual binding mechanism that requires the concurrent engagement of both αvβ3 integrin and c-FMS receptors, which are highly expressed in osteoclasts. Binding to only one of the receptors is markedly less effective [23], thereby reducing off-target effects, such as those on macrophages and other immune cells. (2) The affinity of M-CSF$_{RGD}$ for αvβ3 integrin and c-FMS receptors is lower than that of their natural ligands, vitronectin and M-CSF (CSF-1), respectively [45,49]. We suppose that this lower affinity reduces the likelihood of competing with natural ligands in non-target tissues, minimizing unintended interference with c-FMS signaling in macrophages. (3) Although c-FMS is expressed in Kupffer cells, the resident macrophages in the liver [50,51], our biodistribution studies did not indicate any significant accumulation of M-CSF$_{RGD}$-HSA in the liver. This indicates M-CSF$_{RGD}$-HSA's minimal interaction with c-FMS on Kupffer cells under physiological conditions, further reducing the likelihood of immunosuppressive side effects.

Current catabolic treatments for bone disorders ultimately shift the system toward a lower bone turnover rate [52], and thus cannot be used for a prolonged period of time, which is a major limitation in the treatment of chronic conditions such as osteoporosis. Anabolic treatments strongly promote bone formation, but their efficacy decreases within a year or two of use [53]. Therefore, our approach can be particularly attractive as a treatment alternative for chronic bone conditions such as osteoporosis, where long-term efficacy and safety are of high concern and importance.

3.1. Experimental procedures

3.1.1. Ethics statement

This study was conducted according to protocols approved by the Ben-Gurion University Committee for the Ethical Care and Use of Animals in Experiments (permit number: IL-0401-2019(D)). All surgeries were performed under anesthesia, and all efforts were made to minimize discomfort, distress, and suffering.

3.1.2. Fusion to HSA and protein purification

HSA conjugation to M-CSF$_{RGD}$ was designed at the C-terminal side of M-CSF$_{RGD}$ *via* a short flexible linker (GGGGS). The cloning process was conducted by GenScript (NJ, USA) on the pPICK9K plasmid (Sigma-Aldrich, MO, USA). To introduce the M-CSF$_{c\text{-}FMS}$ into the HSA-containing plasmid, both the gene and vector were digested with *Eco*RI and *Avr*II enzymes (New England Biolabs, MA, USA) and purified from an agarose gel. The digested fragments were ligated and transformed into DH10B competent bacteria. Plasmids were purified using MaxiPrep (Machery-Angel, Germany) and transformed into GS115 *Pichia pastoris* yeast (Sigma-Aldrich, MO, USA) according to the manufacturer's protocol. The purifications of HSA fusion proteins were done using a Jupiter bioreactor (Solaris Biotechnology, Italy). GS115 containing pPICK9K with M-CSF$_{RGD}$-HSA or M-CSF$_{c\text{-}FMS}$-HSA were incubated in 50 ml BMGY overnight and transferred to 500 ml BMGY for an additional overnight incubation. Then, overnight cultures of yeast were added to FM22 media (315 mM KH_2PO_4, 38 mM $(NH_4)_2SO_4$, 6 mM $CaSO_4$, 82 mM K_2SO_4, 240 mM $MgSO_4$, 4 % glycerol, pH = 5.0) and 50 ml of PTM4 (8 mM $CuSO_4$, 0.5 mM NaI, 17 mM $MnSO_4$, 0.8 mM Na_2MoO_4, 0.3 mM H_3BO_3, 3 mM $CaSO_4$, 4 mM $CoCl_2$, 51 mM $ZnCl_2$, 144 mM $FeSO_4$, 0.8 mM biotin, and 0.1 % $H2_SO_4$). Cells were growing under 30 % dO_2 controlled by stirring rpm, air, and O_2 throughput. When glycerol was completely consumed, MeOH was added and adjusted according to the wet cell mass. After three days of fermentation, the media was collected, centrifuged at 4500 rpm for 15 min. 300 mM NaCl and 10 mM imidazole were added to the supernatant, the pH was adjusted to 8.0, and it was incubated for 1 h at 4 °C. The media was centrifuged again and filtered using a 0.22 μm filter (PALL, NY, USA). The filtered media was loaded on a HisTrap™ nickel column (GE Healthcare, MA, USA) using a peristaltic pump. Columns were washed with washing buffer (500 mM NaCl, 10 mM imidazole, 20 mM Na2HPO4, pH = 8.0) and eluted with elution buffer (500 mM NaCl, 300 mM imidazole, 20 mM Na2HPO4, pH = 8.0) on AKTA FPLC (GE Healthcare, MA, USA). Eluted proteins were treated with Endoglycosidase H (New England Biolabs, MA, USA) and separated using a Superdex 200/16/600 column (GE Healthcare, MA, USA). Protein yield was around 30 mg per 1 L of starting culture for all fusion proteins. Protein concentration was determined using an Evolution 260 bio spectrophotometer (Thermo Fisher Scientific, USA) based on protein absorption at 280 nm and the molar extinction coefficient of 49,385 M^{-1} cm^{-1}.

3.1.3. Osteoclast differentiation in vitro

Mouse BMMs were purified and isolated as previously described [23]. After 3 days in alpha Minimum Essential Medium (Sigma-Aldrich, MO, USA) supplemented with 10 % FBS (Sigma-Aldrich, MO, USA), 50,000 units penicillin, 50 mg streptomycin, and 20 ng/ml murine M-CSF (Peprotech, Israel), the cells were detached with a cell scraper. The cells were replated in a 96-well plate (2×10^4 cells/well) in differentiation medium (20 ng/ml) M-CSF and 20 ng/ml RANKL (R&D, MN, USA) and treated with different concentrations of M-CSF$_{RGD}$, M-CSF$_{RGD}$-HSA (50 nM, 250 nM, and 1 μM) or M-CSF$_{c\text{-}FMS}$, M-CSF$_{c\text{-}FMS}$-HSA (50 nM, 1 μM, and 5 μM). The culture medium was changed every two days. After 96 h, cells were fixed with 4 % paraformaldehyde and stained using a TRAP staining kit (Sigma-Aldrich, MO, USA) according to the manufacturer's protocol, with additional staining of the nuclei with DAPI (Sigma-Aldrich, MO, USA). An Olympus IX81 inverted microscope was used to capture twenty random images in each well (at 20× magnification). Thereafter, each image was analyzed manually for osteoclast number, total nuclei number, and total osteoclast area per well in a double-blind manner using ImageJ2 software [54]. An osteoclast was defined as a TRAP-positive cell with three or more nuclei. Each experiment was performed in triplicate, and each condition was normalized to the respective positive control (cells cultured with M-CSF and RANKL).

3.1.4. Biodistribution analysis by in vivo imaging system (IVIS)

M-CSF$_{RGD}$ and M-CSF$_{RGD}$-HSA were conjugated to DyLight 680-NHS Ester (Thermo Scientific, MA, USA), according to the manufacturer's protocol, and washed repeatedly in PBS (Biological Industries, Israel), using a 3.5 kDa cutoff dialysis bag (Generon, UK), followed by several centrifugations with a Vivaspin concentrator (GE Healthcare, MA, USA), until no residual color was seen in the filtrate container.

Thirteen-week-old female BALB/c mice were SC injected with 100 μl of 2 nmol (5 mg/kg) DyLight-conjugated M-CSF$_{RGD}$ or M-CSF$_{RGD}$-HSA. Injection with 100 μl of 2 nmol of DyLight 680-NHS Ester (prepared by incubation in 150 mM Tris for 15 min and dilution to 0.5 mM) served as a control for unspecific binding. The mice were sacrificed at 1, 2, 3, 6, 24, 48, 72, 96, and 168 h post-injection. The internal organs or femurs were extracted and imaged using the Lumina IVIS system (Perkin Elmer, MA, USA), with 1 s of exposure per frame.

3.1.5. Pharmacokinetic analysis

M-CSF$_{RGD}$ (10 mg/kg) was injected IV, and M-CSF$_{RGD}$-HSA (10 mg/kg) was injected either IV or SC into thirteen-week-old female BALB/c mice. The mice were sacrificed after 1, 6, 48, 72, 96, and 168 h ($n = 3$ per group). Blood samples were collected by cardiac puncture, and serum was separated using Minicollect® tubes (Greiner, Germany) according to the manufacturer's protocol.

To measure the serum concentrations of M-CSF$_{RGD}$ and M-CSF$_{RGD}$-HSA, a high-binding 96-well plate (Greiner, Germany) was coated with 2 μg/ml of anti-FLAG antibody (Sigma-Aldrich, MO, USA) in coating buffer (100 mM bicarbonate and 35 mM carbonate pH = 9.5) overnight at 4 °C. Wells were washed three times with PBST (PBS with 0.05 % Tween-20) and blocked with 5 % FBS for 1 h at room temperature. Wells were washed three times, and mouse serum samples were added to the wells in duplicates alongside a standard curve (generated by incubating known concentrations of purified recombinant M-CSF$_{RGD}$-HSA in mouse serum) (Sigma-Aldrich, MO, USA) for 3 h at room temperature. Wells were washed three times and incubated with 0.25 μg/ml of HRP anti-6 × His tag (Abcam, UK) for 2 h at room temperature. For color development, 3,3′,5,5′-Tetramethylbenzidine (TMB) for high M-CSF$_{RGD}$-HSA concentrations or ultra-TMB for low M-CSF$_{RGD}$-HSA concentrations were added for several minutes, followed by a solution of 1 M H_2SO_4 to stop the chromogenic reaction. The plate was imaged using a microplate reader (Biotek, VT, USA) at 450 nm and 650 nm wavelengths. For each well, the background signal at 650 nm was subtracted from the 450 nm signal. Serum concentrations of M-CSF$_{RGD}$ and M-CSF$_{RGD}$-HSA were calculated based on the respective calibration curve.

A graph of serum concentration *vs.* time of M-CSF$_{RGD}$ (IV) and M-CSF$_{RGD}$-HSA (IV and SC) was plotted, and the non-compartmental pharmacokinetic analysis of these data was performed using the PKSolver 2.0 Microsoft Excel add-on [55].

3.2. Ovariectomized mice treatment with M-CSF$_{RGD}$-HSA, M-CSF$_{c\text{-}FMS}$, or alendronate

Thirteen-week-old female BALB/c mice were ovariectomized or sham-operated under complete anesthesia using ketamine (Bremer Pharma, Germany) and xylazine (Phibro, NJ, USA). After the surgery, the mice were allowed to recover for one week while being closely monitored for signs of postoperative pain or distress. Following one week of recovery, ten to twelve mice per group were SC injected with either PBS, M-CSF$_{RGD}$-HSA (2.5 or 10 mg/kg), 10 mg/kg M-CSF$_{c\text{-}FMS}$, or

0.1 mg/kg alendronate (Calbiochem, CA, USA) twice a week for three weeks. On days four and one prior to sacrifice, the mice were IP injected with 10 mg/kg calcein green (Sigma-Aldrich, MO, USA). To exclude mice with abnormal weight loss, the mice were weighted every 3 to 4 days throughout the treatment duration. After the sacrifice, the uteri were extracted and weighted to validate ovariectomy success. Mice with a high uterus-to-body weight ratio were excluded from the experiment. Serum, femurs, tibiae, and vertebrae were collected from each mouse for further evaluation.

3.3. Micro-computed tomography (μCT)

Following sacrifice, vertebrae and right femurs were collected and stored in PBS-soaked gauze prior to imaging. Scanning, thresholding, and analysis were performed as described previously [56]. For vertebrae, trabecular bone parameters were assessed in a region starting 0.76 mm below the superior and above the inferior vertebral endplates. For femurs, an area of 2.2 mm of the midshaft was chosen to analyze the cortical bone.

3.4. Bone turnover markers measurement

Serum was collected *via* cardiac puncture and separated using a Minicollect ® tube (Greiner, Germany) according to manufacturer's protocol. CTX-I levels were evaluated using RatLaps™ (CTX—I) EIA (IDS, UK) according to the manufacturer's protocol. PINP serum levels were measured with Rat/Mouse PINP EIA (IDS, UK) according to the manufacturer's protocol. Hemolyzed serum samples were excluded from the analysis. For each treatment group, ten to twelve samples were analyzed. The concentration of each sample was calculated according to a standard curve prepared according to the manufacturer's protocol.

3.5. Histology

Vertebrae were fixed in 4 % PFA with 0.1 M phosphate buffer for 48 h at room temperature. Next, vertebrae were transferred to 85 mM ethylenediaminetetraacetic acid (EDTA) for three weeks, while replacing the EDTA solution every three days until sufficient decalcification. After that, the bones were washed with increasing concentrations of EtOH, followed by xylene. Bones were embedded in paraffin (Sigma-Aldrich, MO, USA), and the sections (7 μm) were prepared using a Leica microtome (Leica Microsystems, IL, USA). Six slides per treatment group were washed with decreasing concentrations of EtOH and stained for TRAP with acetate buffer (0.2 M $C_2H_3NaO_2$ and 50 mM L (+) tartaric acid) containing 0.5 mg/ml naphthol AS-MX phosphate and 1.1 mg/ml fast red TR salt for 1 h at 37 °C. Sections were imaged with a Zeiss microscope (Zeiss, Germany) and analyzed for bone surface area, osteoclast surface area, and osteoclast number using CaseViewer software (3DHISTECH, Hungary).

3.6. Statistical analysis

The results are reported as the mean ± SD or ±SEM values. Statistically significant differences between the groups were assessed using one-way analysis of variance analysis, followed by Tukey's multiple comparison test. A *p-value* < 0.05 was considered statistically significant.

CRediT authorship contribution statement

Yuval Zur: Writing – original draft, Visualization, Validation, Resources, Methodology, Investigation, Funding acquisition, Formal analysis, Conceptualization. **Svetlana Katchkovsky:** Writing – review & editing, Visualization, Validation, Methodology, Investigation, Formal analysis, Data curation. **Amit Itzhar:** Writing – original draft, Methodology. **Chen-Viki Abramovitch-Dahan:** Project administration, Methodology. **David Stepensky:** Writing – review & editing, Writing – original draft, Visualization, Validation, Methodology, Formal analysis. **Niv Papo:** Writing – review & editing, Writing – original draft, Visualization, Validation, Supervision, Resources, Methodology, Investigation, Funding acquisition, Formal analysis, Conceptualization. **Noam Levaot:** Writing – review & editing, Writing – original draft, Visualization, Validation, Supervision, Resources, Methodology, Investigation, Funding acquisition, Formal analysis, Conceptualization.

Consent to participate

Not applicable.

Consent to publish

All authors agree with the submission and the work has not been published or submitted for publication elsewhere either completely or in part, or in another form or language.

Ethics approval

All mouse studies were conducted according to protocols approved by the Ben-Gurion University Committee for the Ethical Care and Use of Animals in Experiments (permit number: IL-04-01-2019(D)).

Code availability

Not applicable.

Funding

This work was supported by grants from the Israel Science Foundation no. 357/18 (NL) and 1615/19 (NP), the Rosetrees Foundation no. OoR2022\100004 (NP).

Declaration of competing interest

The authors declare that they have no known competing financial interests or personal relationships that could have appeared to influence the work reported in this paper.

Acknowledgements

Not applicable.

During the preparation of this work the authors used [ChatGPT 4o] to aid in language editing. After using this tool, the authors reviewed and edited the content as needed and take full responsibility for the content of the publication.

Appendix A. Supplementary data

Supplementary data to this article can be found online at https://doi.org/10.1016/j.ijbiomac.2024.136821.

Data availability

Data will be made available on reasonable request.

References

[1] D.V. Novack, S.L. Teitelbaum, The osteoclast: friend or foe? Annu. Rev. Pathol. 3 (2008) 457–484, https://doi.org/10.1146/ANNUREV.PATHMECHDIS.3.121806.151431.

[2] N.A. Sims, T.J. Martin, Osteoclasts provide coupling signals to osteoblast lineage cells through multiple mechanisms, Annu. Rev. Physiol. 82 (2020) 507–529, https://doi.org/10.1146/ANNUREV-PHYSIOL-021119-034425.

[3] N. I. of H. NIH, National Institutes of Health (NIH) consensus development panel on osteoporosis prevention, diagnosis, and therapy, Jama 285 (6) (2001) 785–795.
[4] P.D. Miller, Anti-resorptives in the management of osteoporosis, Best Pract. Res. Clin. Endocrinol. Metab. 22 (5) (Oct. 2008) 849–868, https://doi.org/10.1016/J.BEEM.2008.07.004.
[5] D.M. Black, et al., Randomised trial of effect of alendronate on risk of fracture in women with existing vertebral fractures, Lancet 348 (9041) (1996) 1535–1541, https://doi.org/10.1016/S0140-6736(96)07088-2.
[6] C. Fixen, J. Tunoa, Romosozumab: a review of efficacy, safety, and cardiovascular risk, Curr. Osteoporos. Rep. 19 (1) (Feb. 2021) 15–22, https://doi.org/10.1007/S11914-020-00652-W.
[7] S. Minisola, et al., Update on the safety and efficacy of teriparatide in the treatment of osteoporosis, Ther. Adv. Musculoskelet. Dis. 11 (2019), https://doi.org/10.1177/1759720X19877994.
[8] M. Whitaker, J. Guo, T. Kehoe, G. Benson, Bisphosphonates for osteoporosis–where do we go from here? N. Engl. J. Med. 366 (22) (May 2012) 2048–2051, https://doi.org/10.1056/NEJMP1202619.
[9] S. Khosla, et al., Bisphosphonate-associated osteonecrosis of the jaw: report of a task force of the American Society for Bone and Mineral Research, J. Bone Miner. Res. 22 (10) (Oct. 2007) 1479–1491, https://doi.org/10.1359/JBMR.0707ONJ.
[10] G. Karsenty, S. Khosla, The crosstalk between bone remodeling and energy metabolism: a translational perspective, Cell Metab. 34 (6) (Jun. 2022) 805–817, https://doi.org/10.1016/J.CMET.2022.04.010.
[11] E. Shane, et al., Atypical subtrochanteric and diaphyseal femoral fractures: second report of a task force of the American Society for Bone and Mineral Research, J. Bone Miner. Res. 29 (1) (Jan. 2014) 1–23, https://doi.org/10.1002/JBMR.1998.
[12] A.G. Costa, N.E. Cusano, B.C. Silva, S. Cremers, J.P. Bilezikian, Cathepsin K: its skeletal actions and role as a therapeutic target in osteoporosis, Nat. Rev. Rheumatol. 7 (8) (Jun. 2011) 447–456, https://doi.org/10.1038/nrrheum.2011.77.
[13] R.D. Chapurlat, Odanacatib: a review of its potential in the management of osteoporosis in postmenopausal women, Ther. Adv. Musculoskelet. Dis. 7 (3) (2015) 103, https://doi.org/10.1177/1759720X15580903.
[14] A. Mullard, Merck &Co. drops osteoporosis drug odanacatib, Nat. Rev. Drug Discov. 15 (10) (Sep. 2016) 669, https://doi.org/10.1038/NRD.2016.207.
[15] D.L. Lacey, et al., Osteoprotegerin ligand is a cytokine that regulates osteoclast differentiation and activation, Cell 93 (2) (Apr. 1998) 165–176, https://doi.org/10.1016/S0092-8674(00)81569-X.
[16] G. Guterman-Ram, M. Pesic, A. Orenbuch, T. Czeiger, A. Aflalo, N. Levaot, Dual-specificity tyrosine phosphorylation-regulated kinase 2 regulates osteoclast fusion in a cell heterotypic manner, J. Cell. Physiol. 233 (1) (Jan. 2018) 617–629, https://doi.org/10.1002/JCP.25922.
[17] I. Omar, G. Guterman-Ram, D. Rahat, Y. Tabach, M. Berger, N. Levaot, Schlafen2 mutation in mice causes an osteopetrotic phenotype due to a decrease in the number of osteoclast progenitors, Sci. Rep. 8 (1) (Dec. 2018), https://doi.org/10.1038/S41598-018-31428-Z.
[18] W.J. Boyle, W.S. Simonet, D.L. Lacey, Osteoclast differentiation and activation, Nat 423 (6937) (May 2003) 337–342, https://doi.org/10.1038/nature01658.
[19] F.P. Ross, et al., Interactions between the bone matrix proteins osteopontin and bone sialoprotein and the osteoclast integrin alpha v beta 3 potentiate bone resorption, J. Biol. Chem. 268 (13) (1993) 9901–9907, https://doi.org/10.1016/S0021-9258(18)98430-9.
[20] W. Zou, S.L. Teitelbaum, Integrins, growth factors, and the osteoclast cytoskeleton, Ann. N. Y. Acad. Sci. 1192 (1) (Apr. 2010) 27–31, https://doi.org/10.1111/J.1749-6632.2009.05245.X.
[21] K.P. McHugh, et al., Mice lacking β3 integrins are osteosclerotic because of dysfunctional osteoclasts, J. Clin. Invest. 105 (4) (2000) 433–440, https://doi.org/10.1172/JCI8905.
[22] R. Faccio, S. Takeshita, A. Zallone, F.P. Ross, S.L. Teitelbaum, c-Fms and the αvβ3 integrin collaborate during osteoclast differentiation, J. Clin. Invest. 111 (5) (Mar. 2003) 749, https://doi.org/10.1172/JCI16924.
[23] Y. Zur, et al., A dual-specific macrophage colony-stimulating factor antagonist of c-FMS and αvβ3 integrin for osteoporosis therapy, PLoS Biol. 16 (8) (Aug. 2018) e2002979, https://doi.org/10.1371/JOURNAL.PBIO.2002979.
[24] M. J. Knaufs, D. P. Bell, P. Hirtzerq, Z.-P. Luo, J. D. Young, and N. V Katregll, "J. Biol. Chem. Relationship of effective molecular size to systemic clearance in rats of recombinant interleukin-2 chemically modified with water-soluble polymers*," vol. 263, no. 29, pp. 15064–15070, 1388.
[25] Z. Li, B.F. Krippendorff, D.K. Shah, Influence of molecular size on the clearance of antibody fragments, Pharm. Res. 34 (10) (Oct. 2017) 2131, https://doi.org/10.1007/S11095-017-2219-Y.
[26] T. Maack, V. Johnson, S.T. Kau, J. Figueiredo, D. Sigulem, Renal filtration, transport, and metabolism of low-molecular-weight proteins: a review, Kidney Int. 16 (3) (Sep. 1979) 251–270, https://doi.org/10.1038/KI.1979.128.
[27] P.J. Carter, Introduction to current and future protein therapeutics: a protein engineering perspective, Exp. Cell Res. 317 (9) (May 2011) 1261–1269, https://doi.org/10.1016/J.YEXCR.2011.02.013.
[28] P. Chames, M. Van Regenmortel, E. Weiss, D. Baty, Therapeutic antibodies: successes, limitations and hopes for the future, Br. J. Pharmacol. 157 (2) (May 2009) 220, https://doi.org/10.1111/J.1476-5381.2009.00190.X.
[29] J.S. Huston, et al., Protein engineering of antibody binding sites: recovery of specific activity in an anti-digoxin single-chain Fv analogue produced in Escherichia coli, Proc. Natl. Acad. Sci. U. S. A. 85 (16) (1988) 5879, https://doi.org/10.1073/PNAS.85.16.5879.
[30] H.L. Zhao, X.Q. Yao, C. Xue, Y. Wang, X.H. Xiong, Z.M. Liu, Increasing the homogeneity, stability and activity of human serum albumin and interferon-α2b fusion protein by linker engineering, Protein Expr. Purif. 61 (1) (Sep. 2008) 73–77, https://doi.org/10.1016/J.PEP.2008.04.013.
[31] W.F. Richter, B. Jacobsen, Subcutaneous absorption of biotherapeutics: knowns and unknowns, Drug Metab. Dispos. 42 (11) (Nov. 2014) 1881–1889, https://doi.org/10.1124/DMD.114.059238.
[32] W.F. Richter, S.G. Bhansali, M.E. Morris, Mechanistic determinants of biotherapeutics absorption following SC administration, AAPS J. 14 (3) (Sep. 2012) 559–570, https://doi.org/10.1208/S12248-012-9367-0/METRICS.
[33] I. Usach, R. Martinez, T. Festini, J.E. Peris, Subcutaneous injection of drugs: literature review of factors influencing pain sensation at the injection site, Adv. Ther. 36 (11) (Nov. 2019) 2986–2996, https://doi.org/10.1007/S12325-019-01101-6/TABLES/2.
[34] K.L. Stoner, H. Harder, L.J. Fallowfield, V.A. Jenkins, Intravenous versus subcutaneous drug administration. which do patients prefer? A systematic review, Patient - Patient-Centered Outcomes Res. 8 (2) (Jul. 2014) 145–153, https://doi.org/10.1007/S40271-014-0075-Y.
[35] "Drug Approval Package: Fosamax(Alendronate Sodium) NDA# 20560/S013." https://www.accessdata.fda.gov/drugsatfda_docs/nda/99/020560S13_Fosamax.cfm (accessed Sep. 09, 2022).
[36] R. Samadfam, Q. Xia, D. Goltzman, Co-treatment of PTH with osteoprotegerin or alendronate increases its anabolic effect on the skeleton of oophorectomized mice, J. Bone Miner. Res. 22 (1) (Jan. 2007) 55–63, https://doi.org/10.1359/JBMR.060915.
[37] R. Samadfam, Q. Xia, D. Goltzman, Pretreatment with anticatabolic agents blunts but does not eliminate the skeletal anabolic response to parathyroid hormone in oophorectomized mice, Endocrinology 148 (6) (Jun. 2007) 2778–2787, https://doi.org/10.1210/EN.2006-1475.
[38] H. Yamane, A. Sakai, T. Mori, S. Tanaka, K. Moridera, T. Nakamura, The anabolic action of intermittent PTH in combination with cathepsin K inhibitor or alendronate differs depending on the remodeling status in bone in ovariectomized mice, Bone 44 (6) (Jun. 2009) 1055–1062, https://doi.org/10.1016/J.BONE.2008.05.010.
[39] L. Song, et al., Optimization of the time window of interest in ovariectomized imprinting control region mice for antiosteoporosis research, Biomed. Res. Int. 2017 (2017) 1–10, https://doi.org/10.1155/2017/8417814.
[40] K. Ishida, M. Yamaguchi, Role of albumin in osteoblastic cells: enhancement of cell proliferation and suppression of alkaline phosphatase activity, Int. J. Mol. Med. (Dec. 2004), https://doi.org/10.3892/ijmm.14.6.1077.
[41] D.B. Horváthy, et al., Serum albumin as a local therapeutic agent in cell therapy and tissue engineering, BioFactors 43 (3) (May 2017) 315–330, https://doi.org/10.1002/biof.1337.
[42] J. Nilsen, et al., Human and mouse albumin bind their respective neonatal Fc receptors differently, Sci. Report. 8 (1) (Oct. 2018) 1–12, https://doi.org/10.1038/s41598-018-32817-0.
[43] C. Chaudhury, et al., The major histocompatibility complex-related fc receptor for IgG (FcRn) binds albumin and prolongs its lifespan, J. Exp. Med. J. Exp. Med. 197 (3) (2003) 315–322, https://doi.org/10.1084/jem.20021829.
[44] J.P. Doweiko, D.J. Nompleggi, Reviews: role of albumin in human physiology and pathophysiology, J. Parenter. Enter. Nutr. 15 (2) (Mar. 1991) 207–211, https://doi.org/10.1177/0148607191015002207.
[45] J. Elegheert, et al., Allosteric competitive inactivation of hematopoietic CSF-1 signaling by the viral decoy receptor BARF1, Nat. Struct. Mol. Biol. 19 (9) (Aug. 2012) 938–947, https://doi.org/10.1038/nsmb.2367.
[46] P. D'Amelio, et al., Alendronate reduces osteoclast precursors in osteoporosis, Osteoporos. Int. 21 (10) (Dec. 2009) 1741–1750, https://doi.org/10.1007/S00198-009-1129-1.
[47] E.R. Van Beek, C.W.G.M. Löwik, S.E. Papapoulos, Effect of alendronate treatment on the osteoclastogenic potential of bone marrow cells in mice, Bone 20 (4) (Apr. 1997) 335–340, https://doi.org/10.1016/S8756-3282(97)00006-9.
[48] P.R. Jensen, T.L. Andersen, P. Chavassieux, J.P. Roux, J.M. Delaisse, Bisphosphonates impair the onset of bone formation at remodeling sites, Bone 145 (Apr. 2021) 115850, https://doi.org/10.1016/J.BONE.2021.115850.
[49] Laura Belvisi, et al., Potent integrin antagonists from a small library of RGD-including cyclic pseudopeptides, Org. Lett. 3 (7) (2001) 1001–1004.
[50] T.G. Douglass, et al., Macrophage colony stimulating factor: not just for macrophages anymore! A gateway into complex biologies, Int. Immunopharmacol. 8 (10) (Oct. 2008) 1354–1376, https://doi.org/10.1016/j.intimp.2008.04.016.
[51] A. Sehgal, K.M. Irvine, D.A. Hume, Functions of macrophage colony-stimulating factor (CSF1) in development, homeostasis, and tissue repair, Semin. Immunol. 54 (Apr. 2021) 101509, https://doi.org/10.1016/j.smim.2021.101509.
[52] B.L. Riggs, A.M. Parfitt, Drugs used to treat osteoporosis: the critical need for a uniform nomenclature based on their action on bone remodeling, J. Bone Miner. Res. 20 (2) (Nov. 2004) 177–184, https://doi.org/10.1359/JBMR.041114.
[53] L. Bandeira, E.M. Lewiecki, Anabolic therapy for osteoporosis: update on efficacy and safety, Arch. Endocrinol. Metab. 66 (5) (Nov. 2022) 707–716, https://doi.org/10.20945/2359-3997000000566.
[54] J. Schindelin, et al., Fiji: an open-source platform for biological-image analysis, Nat. Methods 9 (7) (2012) 676–682.
[55] Y. Zhang, M. Huo, J. Zhou, S. Xie, PKSolver: an add-in program for pharmacokinetic and pharmacodynamic data analysis in Microsoft Excel, Comput. Methods Prog. Biomed. 99 (3) (Sep. 2010) 306–314, https://doi.org/10.1016/J.CMPB.2010.01.007.
[56] S. Katchkovsky, B. Chatterjee, C.-V. Abramovitch-Dahan, N. Papo, N. Levaot, Competitive blocking of LRP4–sclerostin binding interface strongly promotes bone anabolic functions, Cell. Mol. Life Sci. 79 (2) (Feb. 2022) 113, https://doi.org/10.1007/s00018-022-04127-2.